Journal of Hazardous Materials 297 (2015) 329–339

Contents lists available at ScienceDirect

Journal of Hazardous Materials

journal homepage: www.elsevier.com/locate/jhazmat

Iterative ensemble Kalman filter for atmospheric dispersion in nuclear accidents: An application to Kincaid tracer experiment

X.L. Zhang[a], G.F. Su[a], J.G. Chen[a], W. Raskob[b], H.Y. Yuan[a,*], Q.Y. Huang[a]

[a] Institute of Public Safety Research, Department of Engineering Physics, Tsinghua University, Beijing 100084 PR China
[b] Institute for Nuclear and Energy Technologies, Karlsruhe Institute of Technology, Karlsruhe, D-76021, Germany

HIGHLIGHTS

- We integrate the iterative EnKF method into the POLYPHEMUS platform.
- We thoroughly evaluate the data assimilation system against the Kincaid dataset.
- The data assimilation system substantially improves the model predictions.
- More than 60% of the retrieved emissions are within a factor two of actual values.
- The results reveal that the boundary layer height is the key influential factor.

ARTICLE INFO

Article history:
Received 19 January 2015
Received in revised form 13 April 2015
Accepted 19 May 2015
Available online 22 May 2015

Keywords:
Iterative ensemble Kalman filter
Emission estimate
Atmospheric dispersion prediction
Kincaid tracer experiment
Nuclear power plant accident

ABSTRACT

Information about atmospheric dispersion of radionuclides is vitally important for planning effective countermeasures during nuclear accidents. Results of dispersion models have high spatial and temporal resolutions, but they are not accurate enough due to the uncertain source term and the errors in meteorological data. Environmental measurements are more reliable, but they are scarce and unable to give forecasts. In this study, our newly proposed iterative ensemble Kalman filter (EnKF) data assimilation scheme is used to combine model results and environmental measurements. The system is thoroughly validated against the observations in the Kincaid tracer experiment. The initial first-guess emissions are assumed to be six magnitudes underestimated. The iterative EnKF system rapidly corrects the errors in the emission rate and wind data, thereby significantly improving the model results (>80% reduction of the normalized mean square error, $r = 0.71$). Sensitivity tests are conducted to investigate the influence of meteorological parameters. The results indicate that the system is sensitive to boundary layer height. When the heights from the numerical weather prediction model are used, only 62.5% of reconstructed emission rates are within a factor two of the actual emissions. This increases to 87.5% when the heights derived from the on-site observations are used.

1. Introduction

China is experiencing a rapid expansion of its nuclear power industry. However, the Fukushima accident reminds us that we must be prepared for such devastating nuclear power plant (NPP) accidents and any other accidents where hazardous material is released into the atmosphere. A reliable assessment of atmospheric dispersion of radionuclides is vitally important for population sheltering and evacuation planning during NPP accidents [1–3]. Results of dispersion models [4] may have high spatial and temporal resolutions, but they are not accurate enough due to the insufficient information of source term [5,6] and the large uncertainties in meteorological data [7–9], especially in the critical early stages. Environmental measurements are more reliable, but they are scarce and unable to give information about the future situation. As a result, the substantial uncertainties in radioactive pollution distribution in the atmosphere significantly hinder the decision makers from planning accurate countermeasures.

The combination of model results and environmental measurements can help improve the accuracy of model results and reconstruct the emissions. Inverse modeling and data assimilation (DA) are two main combination methods. Inverse modeling mainly aims at the reconstruction of model parameters. Data assimilation method can sequentially correct the errors of model results and retrieve the model parameters. DA method is used in this study. Data assimilation has been widely used in numerical weather

* Corresponding author. Tel.: +86 10 62792856; fax: +86 10 62792863.
E-mail address: hy-yuan@outlook.com (H.Y. Yuan).

http://dx.doi.org/10.1016/j.jhazmat.2015.05.035
0304-3894/

prediction (NWP) over the past two decades [10]. The DA method has been introduced into the nuclear emergency response system during the past decade [11–16]. In the real time on-line decision support system (RODOS) [17] for European off-site nuclear emergency management, Kalman filter method [18] has been used to improve predictions of Gaussian plume model under quasi-steady state [11–13], and efforts [14–16] were subsequently made to reconstruct source terms. The sequential assimilation method of ensemble Kalman filter (EnKF) [19] is a powerful alternative for nuclear power plant emergency management. It has such advantages as efficient on-line calibration, relatively straightforward implementation and superior scalability for parallel computing. Furthermore, EnKF can simultaneously account for the various uncertainties in both emissions and meteorological data. Recently, Zheng et al. [20–22] has applied the Monte Carlo dispersion model combined with EnKF to reconstruct the source release rate for short range dispersion. However, the performance of EnKF usually deteriorates due to the nonlinear observational model, which relates the state variables (radioactive contents and positions of each puff) to the observations (concentrations). The linear update in EnKF may lead to inaccurate estimates where information in measurements is not utilized maximally. It takes several hours for the DA method to minimize the uncertainties of a priori parameters and converge to the actual values (e.g., in [20]). Recently, Lorentzen and Naevdal [23] have introduced an iterative extension to the ensemble Kalman filter in the field of automatic control. Iterations are introduced to improve the estimates in the cases where the observation model is not linear. The new iterative EnKF method has been successfully applied in the data assimilation system for NPP accidents [24]. The results of twin experiments in our previous study indicate that the proposed iterative EnKF scheme effectively calibrates the errors in emission rate, plume rise height, wind speed and wind direction, and time delay of the EnKF is substantially alleviated. However, the twin experiments only theoretically assess the algorithmical capabilities and improvements of the iterative EnKF method, and it can be interpreted as optimistic since the further complications of errors in real-life scenario are ignored. The proposed methods should be further evaluated using experimental data. And the meteorological input data can be provided to models by detailed on-site observations if available. But these observations may not be fully available during NPP accidents, so the data from numerical weather prediction (NWP) is used as substitutes. The influences of NWP data should also be assessed.

The objective of this study is to thoroughly evaluate our proposed iterative EnKF data assimilation scheme in [24] with the data from Kincaid tracer experiment [25], which involves highly buoyant plumes. The errors in the horizontal wind will be corrected and the emission rates will be reconstructed using the iterative EnKF method. Only the measured ground level tracer (SF_6) concentrations are assimilated by the system. The influences of input meteorological data on the data assimilation performance are also investigated, by comparison of the results driven by both the weather research and forecasting (WRF) predicted and on-site observed meteorological data, as suggested in [26]. We also try to ascertain the most influential meteorological parameter in determining the sensitivity and accuracy of the data assimilation system, and to provide suggestions for the practical implication of this method.

2. Material and methods

2.1. Kincaid experiments and observations

The Kincaid field experiment was performed as part of the EPRI Plume Model Validation and Development Project [25,27]. A comprehensive experimental campaign was conducted at the Kincaid power plant (39.59°N, 89.49°W), Illinois, USA, in 1980 and 1981. The power plant was surrounded by flat farmland with some lakes, as shown in Fig. 1. During the experiment, SF_6 was released from the 187 m high plant stack of 9 m diameter. One-hour averaged ground level concentrations were measured. The data used for the following simulations is given with the model validation kit (http://www.harmo.org/kit/). In this study, the data from the experiment conducted on July 13, 1980, between 9:00 and 17:00 GMT-6, is used. The actual mean emission rate in the experiment is 13.36 g s^{-1}, with a standard deviation of 1.05 g s^{-1}. The layout of monitoring network is shown in Fig. 1. There are 162 monitors, ranging between 0.5 km and 15 km from the source. The experiment has 1195 effective surface concentration observations. The observation errors are set as 10% of the observed values.

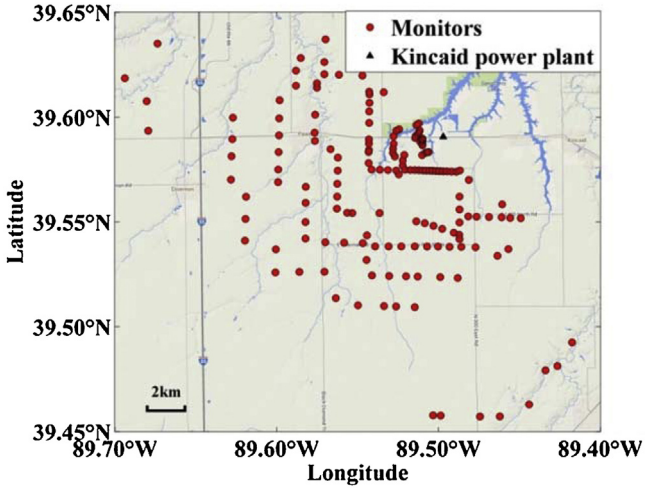

Fig. 1. The computational domain, SF_6 release point (black triangle), and surface measurement network of SF_6 concentration (red dots, 162 stations). (For interpretation of the references to color in this figure legend, the reader is referred to the web version of this article.)

2.2. Dispersion model description

The state and observation of an atmospheric dispersion system can be expressed as

$$x_k = M(x_{k-1}) + \eta,\ x,\ \eta \in \mathrm{R}^n \quad (1)$$

$$y_k^0 = H(x_k) + \epsilon,\ y^0,\ \epsilon \in \mathrm{R}^m \quad (2)$$

where $\boldsymbol{x}$ is the state vector of the dynamic system, n is the length of the state vector, and the subscript k or $k-1$ represents the time step of data assimilation. $M(x)$ is the dispersion model, η is the model error, y^0 is the observation vector, m is the number of the observations, $H(x)$ is observation model, and $\boldsymbol{\epsilon}$ is the measurement error. The dispersion model is Lagrangian puff-model, the same as in [24]. A continuous release is modeled by the release of a discrete set of ellipsoidal clouds with Gaussian density distribution called "puffs". N_{puff} indicates the total number of the released puffs. Each of the puffs carries away some content of hazardous material (Q), and the central position of the puff can be expressed as (x, y, z). In this study, the content Q and horizontal position (x, y) of each puff comprise the state vector of the Lagrangian puff-model, so the length of the state vector is $n = 3\ N_{\mathrm{puff}}$. The heights of puffs were also included in the state vector in [24], but the twin experiments have shown that the reconstructed emission rates and plume rise heights are simultaneously underestimated or overestimated. It is due to the error compensating effect of the two parameters: underestimated release rate reduces the ground level concentration, but

Table 1
Experiments to evaluate the performance of the iterative EnKF data assimilation scheme.

Experiment name	Plume rise/dispersion parameterization	Meteorological data	Whether with DA and source term estimation	Source term	A priori emission rate ($g\,s^{-1}$)
WRF-NoDA	Concawe model/similarity theory	WRF forecast	No	Actual	/
WRF-DA		WRF forecast	Yes	Uncertain	10^{-5}
Obs-NoDA		Measurement	No	Actual	/
Obs-DA		Measurement	Yes	Uncertain	10^{-5}

the lower rise height increases it, and *vice versa*. The two different errors compensate each other, and different combinations of these parameters give similar ground level concentration. It will be difficult for EnKF to identify which one is the optimal solution [20]. The problem becomes more significant when using experimental data. In the following data assimilation experiments, since the a *priori* emission is assumed to be underestimated, the plume rise height always decreases and converges to the height of the source (189 m) to make the predicted ground concentration higher and closer to the observations. The reconstructed emission rates are thereby underestimated due to the error compensating effect. The heights and emission rates are not effectively simultaneously corrected. Fortunately, the plume rise height can also be estimated based on the temperature and velocity of the released plume, which can be measured using remote, non-contact measuring technologies, e.g., infrared technology. As a result, in this study only the errors in the horizontal wind are corrected and the emission rates are reconstructed. The measurements are the ground level volumetric activity concentrations, and the observation model $H(\boldsymbol{x})$ is nonlinear.

In this study, the dispersion simulations of SF_6 are conducted using the Lagrangian puff model [28] of the POLYPHEMUS platform [29]. The Lagrangian puff module has been updated to make it continuously driven by the spatially and temporally evolving meteorological data, which is updated every 10 min. It is assumed that the meteorological data temporally remains constant during this short time period. The time step between two successive puffs is 10 s. The concentration observations are assimilated into the model every hour during the experiment. As shown in Table 1, four experiments were conducted to evaluate the performance of the iterative EnKF scheme, and the influences of different meteorological data. The a *priori* emission rates in our DA runs are all set as $10^{-5}\,g\,s^{-1}$. The Concawe model [30] is adopted as the plume rise parameterization scheme, and similarity theory [31] as the dispersion parameterization scheme. The dispersion system works offline, and it is not coupled with the meteorological model.

2.3. Meteorological data

In this study, both the meteorological data predicted by the weather research and forecasting (WRF, version 3.1) [32], and the on-site observed data are used to investigate the influences of the different meteorological data.

(1) *WRF forecasts*

Four-level nested computational domains (Domain 0 ~ 3) are used, as shown in Fig. 2. The main objective is to obtain meteorological predictions with a spatial resolution of approximately 1 km in the area around the Kincaid power plant, which is in the innermost nested domain. The computational domain shown in Fig. 1 is located in Domain 3. The configurations of the WRF prediction are displayed in Table 2. WRF simulation is initialized with NCEP/NCAR Reanalysis 1 data [33]. The WRF simulation starts at 18:00 GMT-6, July 12, which is 15 h before the initial release of SF_6, and lasts through to 00:00 GMT-6, July 14. WRF is set as parallel mode. The WRF simulation was conducted on our cluster server, which has Intel Xeon E5630 2.53 GHz processors (4–core), 16 nodes (8 cores per node), and 64 GB memory. Two nodes (16 cores) were used, and it took about 2 h to complete the calculation (meteorological data for 30 h). The dispersion simulations start at the initial release time and last through to 17:00 GMT-6, July 13. Two simulations are conducted—one assimilates SF_6 observations via iterative EnKF with an unknown and uncertain initial SF_6 emission rate (WRF-DA in Table 1), whereas the other is free running (i.e., without assimilation) but uses the actual (known) SF_6 emission rates (WRF-NoDA).

(2) *Meteorological measurements*

During the experiment, most meteorological measures were hourly averaged, and taken from a "Central Site" located around 650 m east of the Kincaid plant. Observations of wind speed and wind direction are available at 10, 30, 50 and 100 m, measured by the 100 m and 10 m meteorological towers. Following the preprocessing methods in [26], the horizontal velocity components under 100 m are obtained from the measurements or interpolations, and they are fixed at 100 m values at higher levels. The vertical velocity component is assumed to be zero. Solar radiation data is also available, measured by solar and terrestrial radiation equipment. The Monin–Obukhov length (L), the friction velocity (u_*), and the boundary layer depth (h) derived by Earth Tech using preprocessing methods detailed in [25] are adopted.

(3) *Meteorological data comparisons*

In Fig. 3, the WRF predicted wind speed and wind direction are compared with the measurements. The WRF predictions are linearly interpolated at the "Central Site", where measurements were taken. The solid lines are the temporal trajectory of the predictions. The predictions are averaged in each hour to compare with the hourly averaged measurements. The error bar is the standard deviation of the predictions in each hour. The predicted wind speed captures the overall temporal evolution of the observations: high early on and then relatively steady at a lower speed. The mean absolute deviation between the predictions and observations is 0.27 $m\,s^{-1}$ (maximum: 0.57 $m\,s^{-1}$). The deviations between the predicted wind directions and the observations are larger. The mean absolute deviation is 19.51°, and the maximum deviation amounts to 47 degrees during 16:00–17:00 GMT-6. The large deviation can be caused by the low quality of the initial condition of WRF, namely the reanalysis data. In 1980s, the meteorological observations were limited, which would lead to the relatively low quality of the reanalysis data for that period. The large deviations of the wind

Table 2
Configurations and physical parameterizations of the WRF model.

Configuration parameters	Domain			
	0	1	2	3
Spatial resolution	27 km	9 km	3 km	1 km
Number of grid points	181 × 161	91 × 91	91 × 91	91 × 91
Number of vertical levels	28	28	28	28
Numerical time-step	120 s	60 s	30 s	15 s
Planetary boundary layer	YSU PBL scheme [34]			
Microphysics	WRF Single Moment 3 scheme 35]			

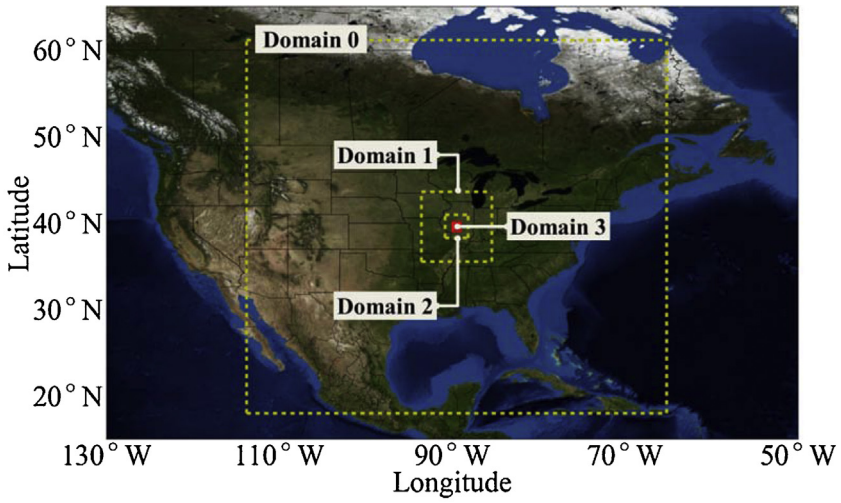

Fig. 2. WRF four-level nested computational domains. The yellow dashed lines are the boundaries of Domain 0 ~2. The red solid lines are the boundaries of innermost Domain 3. (For interpretation of the references to color in this figure legend, the reader is referred to the web version of this article.)

direction will cause distinctly different ground level distributions of SF_6.

2.4. Iterative ensemble Kalman filter

Ensemble Kalman filter (EnKF) [19] is a sequential data assimilation method, which is used recursively to produce a statistically optimal estimate of the underlying system state by merging the model predictions and the current observations. Different from the original Kalman filter, which is only applicable to linear system model, the EnKF initializes an ensemble of forecast models, each of which represents a possible state of the system and the error statistics are predicted using the collection of model states. The ensemble state vectors constitute the state matrix:

$$X = (x_1 x_2 \ldots x_N) \in \mathrm{R}^{n \times N} \tag{3}$$

where the subscript i (i = 1, 2, ..., N) denotes the individual state vector of the ensemble and N denotes the size of the ensemble. EnKF is also applicable to nonlinear system models. The ensemble predictions constitute the prediction matrix, defined as

$$Y^f = \left(H(x_1^f)H(x_2^f)\ldots H(x_N^f)\right) \in \mathrm{R}^{m \times N} \tag{4}$$

$$\bar{Y^f} = Y^f 1_N \tag{5}$$

where 1_N is $N \times N$ matrix, with each element equaling to $1/N$, and $\bar{Y}^f$ is the mean ensemble measurement prediction matrix. For the nonlinear observation operators, the state vector can be extended to include both the original vector $\boldsymbol{x}$ and the observation predictions $H(\boldsymbol{x})$ as in [36], thus the nonlinear problem is reduced to a linear one. But the analysis result is only an approximation to the optimal estimate of the state, because the valid states of system only occupy a submanifold of augmented state space instead of the whole space [36], causing the performance of EnKF to deteriorate. It is found that in [20], when nonlinear parameters (wind direction and turbulence intensity) are included in the state vector, it takes several data assimilation steps to converge to the true values. The time delay between a priori and the converged values can be as large as 5 h.

In the original EnKF, the analysis step is conducted only once, which is insufficient for the nonlinear observation model. The linear update in EnKF may lead to inaccurate estimates where information in measurements is not utilized maximally. In the modified algorithm, an iteration cycle is introduced, which makes the posterior state gradually converge to the actual condition. In the iterative EnKF, there are three main modifications: convergence criterion, increment filter, and resample. The details about the iterative EnKF data assimilation method can be found in [24]. The iterative EnKF scheme has been integrated into the POLYPHEMUS platform [29]. The configurations of the iterative EnKF are the same as those in [24]. The data assimilation system is set as serial mode. All the dispersion simulations and data assimilation were conducted on the personal computer, which has Intel i5-3230 M 2.60 GHz processor, and 6 GB memory. It took about 20 min for the 8 h (from 9:00 to

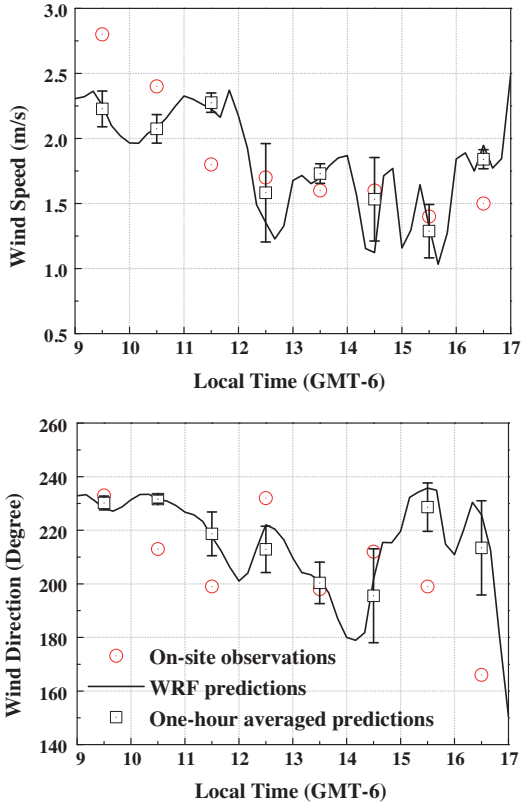

Fig. 3. Comparisons between the WRF predictions and on-site observations: (upper panel) comparison of wind speed and (bottom panel) comparison of wind direction.

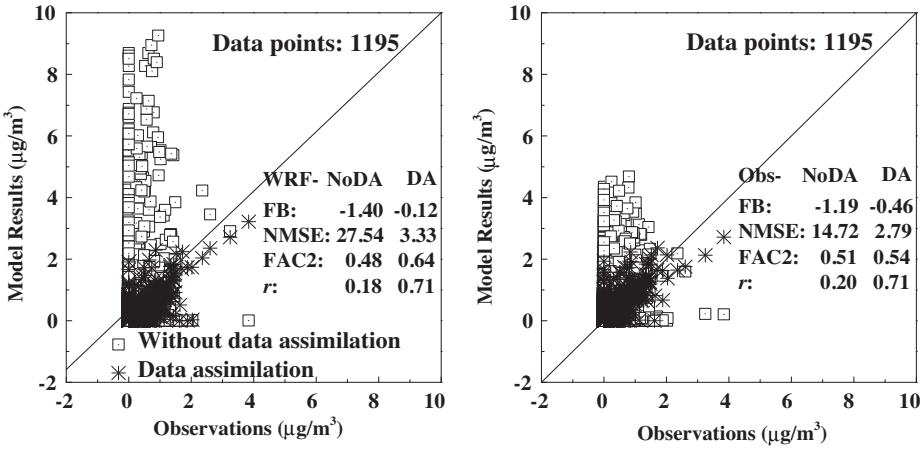

Fig. 4. Scatter plots of observed versus model forecasted surface SF_6 concentration: (left) simulations driven by the WRF predicted meteorological data (WRF-NoDA and WRF-DA); (right) simulations driven by the observed meteorological data (Obs-NoDA and Obs-DA).

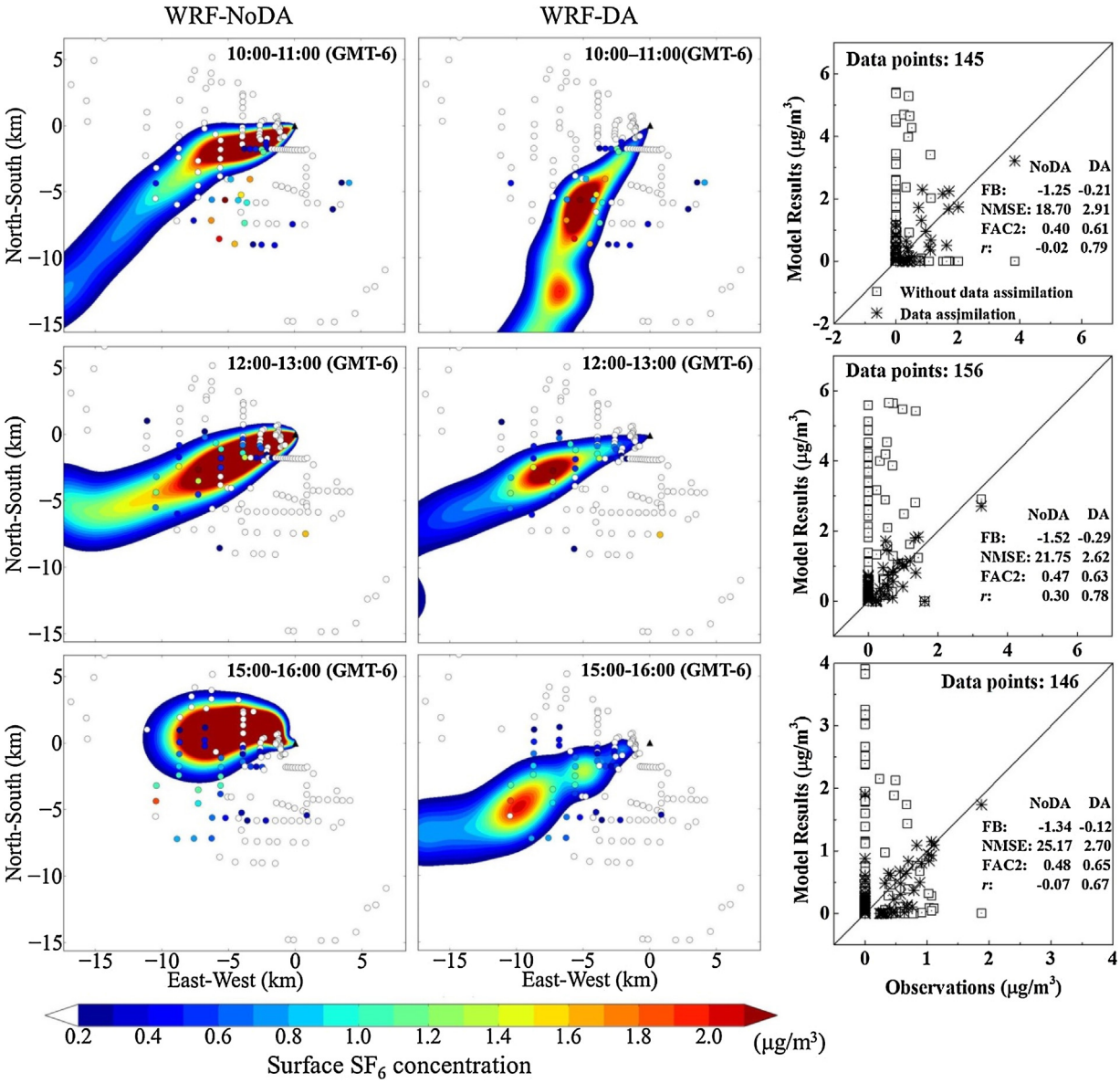

Fig. 5. Forecasts and data assimilation analysis driven by the WRF predicted meteorological data: (First column) Model forecasts with the actual known emissions but without data assimilation (WRF-NoDA); (Second column) data assimilation analysis with unknown and uncertain emissions (WRF-DA); (Third column) scatter plots of model results versus observed surface SF_6 concentrations.

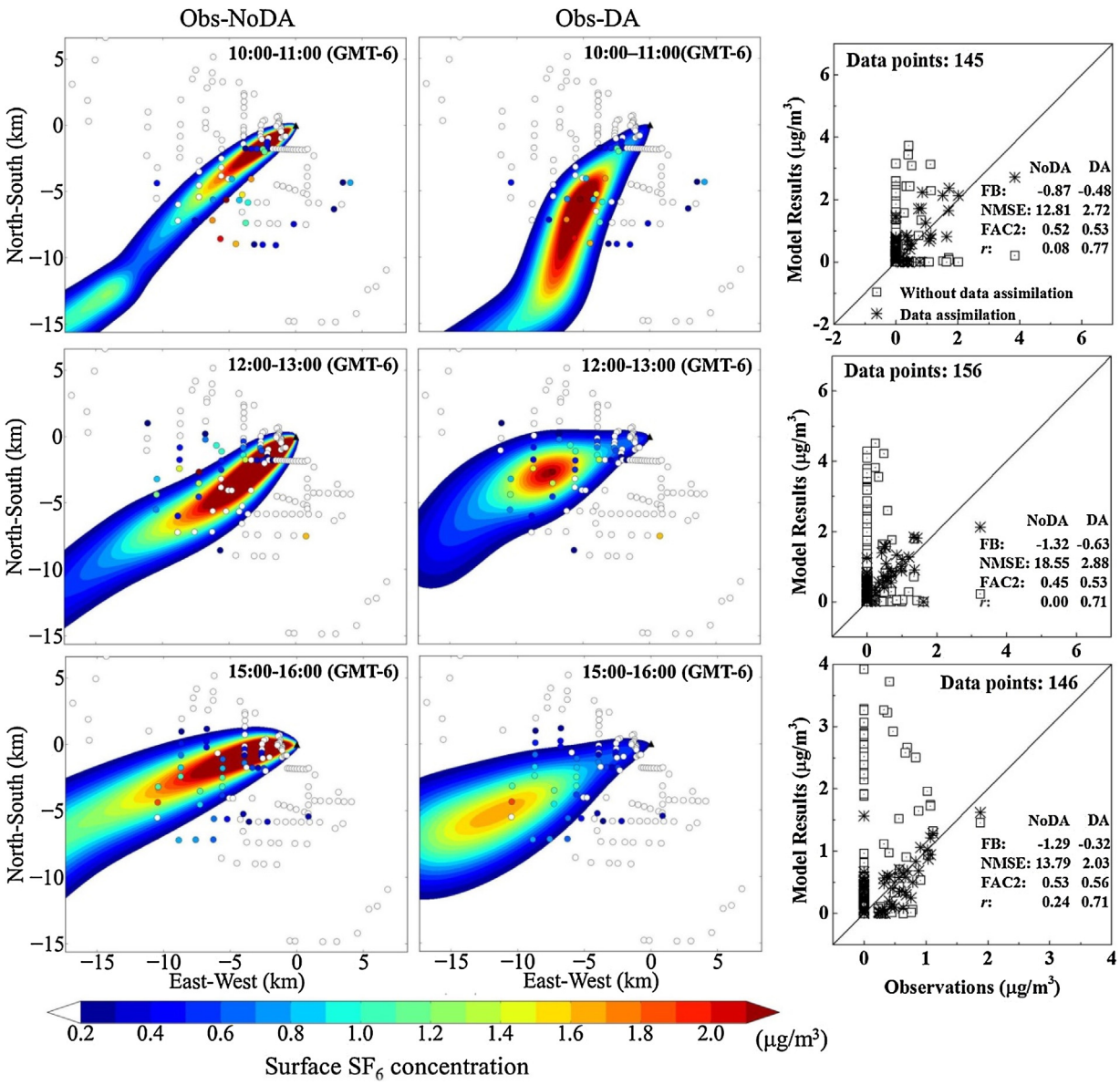

Fig. 6. Forecasts and data assimilation analysis driven by the on-site observed meteorological data: (First column) Model forecasts with the actual known emissions but without data assimilation (Obs-NoDA); (Second column) data assimilation analysis with unknown and uncertain emissions (Obs-DA); (Third column) scatter plots of model results versus observed surface SF_6 concentrations.

11:00) data assimilation runs (WRF-DA or Obs-DA), and it only took less than 3 min for each time of data assimilation on average.

3. Results and discussions

3.1. Assimilation quality

Four statistical metrics are used to quantify the performance of the data assimilation: fractional bias (FB), normalized mean square error (NMSE), fraction of the predictions within a factor two of observations (FAC2) and correlation coefficient (r), following [28]. FB and NMSE are defined as:

$$\mathrm{FB} = \left(\bar{C}_{\mathrm{obs}} - \bar{C}_{\mathrm{assim}}\right) / \left(0.5(\bar{C}_{\mathrm{obs}} + \bar{C}_{\mathrm{assim}})\right) \quad (6)$$

$$\mathrm{NMSE} = (C_{\mathrm{obs}} - \bar{C}_{\mathrm{assim}})^2 / (\bar{C}_{\mathrm{obs}}\bar{C}_{\mathrm{assim}}) \quad (7)$$

where C_{obs} is the concentration observations and C_{assim} is the analysis results after data assimilation. The same metrics are also applied to quantify the performance of the model forecast without data assimilation.

The iterative EnKF scheme can effectively assimilate the observations. Fig. 4 is a scatter plot of model simulated SF_6 surface concentrations, with and without data assimilation, against the observations. The left panel shows the results of the simulations driven by the WRF predictions (WRF-NoDA and WRF-DA). Despite using the actual emission rates, the results in WRF-NoDA show a substantial bias (FB = −140%), a large error (NMSE = 27.54), and a weak correlation (r = 0.18), with only 48% of the forecast SF_6 concentrations within a factor of two of the observations. But in WRF-DA, the iterative EnKF data assimilation scheme substantially reduces the bias (FB = −12%) and error (NMSE = 3.33) and increases the correlation (r = 0.71), with 64% of the analysis SF_6 concentrations within a factor two of the observations. The model results in the right panel are from the simulations driven by the meteorological observations (Obs-NoDA and Obs-DA). They also show that the data assimilation scheme effectively improves the model results.

The results in Obs-NoDA are better than those in WRF-NoDA: the overestimation of the model forecast is slightly alleviated (FB = −119%), the errors are substantially reduced (NMSE = 14.72), the correlation becomes a little stronger (r = 0.20), and more forecast concentrations locate within a factor two of the observations (FAC2 = 0.51). The different forecast performance is caused by the substantial differences between the predicted and observed wind speed and direction as shown in Fig. 3. However, there are still significant biases between the observed and forecast SF_6 concentrations, despite using the observed meteorological data. One plausible reason is that the measurements of wind are one-hour averaged, but the actual wind constantly varied during the measurement period, introducing representativeness errors. The EnKF assimilation also substantially improves the performance, as the statistical metrics indicate.

3.2. Corrections of errors in wind

Fig. 5 shows the SF_6 surface concentrations in WRF-NoDA (first column) and in WRF-DA (second column) during three different periods. There are significant performance improvements in WRF-DA during all the three time periods. The locations or directions of the SF_6 plume are substantially corrected by the iterative EnKF scheme. During the first time period, the forecast plume in WRF-NoDA locates to the west of the source, whereas many high concentrations are observed in the southwest direction relative to the source. It suggests that substantial errors exist in the predicted wind direction. In WRF-DA, the plume is "turned" anticlockwise. The high concentration area of the plume is in good agreement with the observations. The substantial performance improvement can be quantitatively identified from the statistical metrics shown in the third column. During the first time period, the concentrations are dramatically overestimated in WRF-NoDA (FB = −114%, NMSE = 18.70). The forecast and the observations become anti-correlated (r = −0.02). WRF-DA, in contrast, greatly reduces the bias (FB = −21%), increases the correlation between the analysis and observed SF_6 (r = 0.79), and lowers the error (NMSE = 2.91). The differing distributions of model predicted and observed plumes indicate that meteorological errors are a significant part of the transport errors. The situations of the other two periods are similar to that during the first period. The results suggest that the iterative EnKF assimilation effectively and efficiently 'calibrates' the transport error caused by the errors in the predicted wind data.

Fig. 6 shows the same results from the simulations driven by the observed meteorological data. Generally speaking, the forecast in Obs-NoDA outweighs its counterpart in Fig. 5, which is consistent with the results in Fig. 4. After data assimilation, the positions of the SF_6 plume become close to those in Fig. 5, but the plumes are slightly wider in the simulation driven by observed meteorological data due to the larger puff standard deviations, which are calculated according to the Monin–Obukhov similarity theory. Fig. 7 shows the time evolution of the correlation coefficient (r) and NMSE of the forecast SF_6 concentrations versus the observations. For the forecasts without DA, the correlation coefficients in both WRF-NoDA and Obs-NoDA are significantly small (mean = 0.10, maximum = 0.42, minimum = −0.18 in WRF-NoDA, and mean = 0.17, maximum = 0.41, minimum = 0 in Obs-NoDA). The correlation coefficients in Obs-NoDA are higher than those in WRF-NoDA due to the observed meteorological data. But the fluctuations of the correlation coefficients (r) in both of the forecasts are substantially large. The standard deviations of r are respectively 0.24 in WRF-NoDA and 0.17 in Obs-NoDA. In contrast, after DA the data assimilation analysis performs considerably better during 9:00–17:00 as evident in the relatively steady large correlation coefficient (mean = 0.69, maximum = 0.79, minimum = 0.60 in WRF-DA, and mean = 0.69, maximum = 0.77, minimum = 0.47 in Obs-DA). The statistical metrics NMSE also shows similar results. Despite using different meteorological data, after DA the two sets of r and NMSE in WRF-DA and Obs-DA become comparable (within 10% on average in r, and within 18% on average in NMSE). The results indicate that the iterative EnKF scheme effectively calibrate the errors in the wind data.

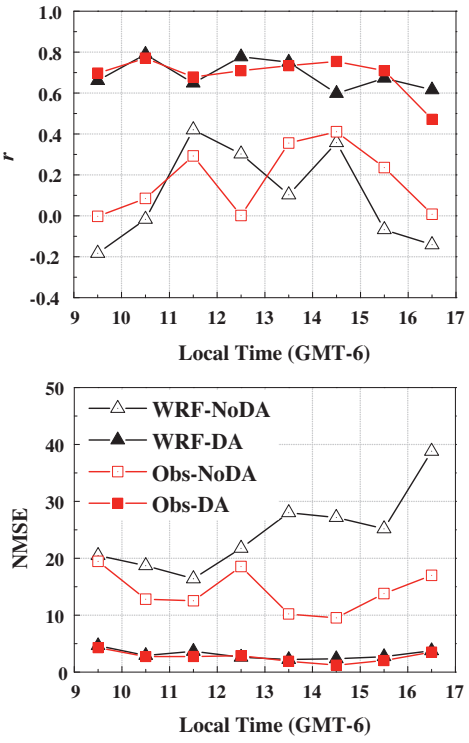

Fig. 7. Correlation coefficient (top) and normalized mean square error (bottom) between observed and model results (with and without assimilation) surface SF_6 concentrations.

3.3. Emission rate reconstruction

It takes about three hours for the puff to leave the computational area, so the emission estimations can be updated three times on average. Here, the mean and standard deviation (error bar) of the multiple updates of the emission are shown. Fig. 8 shows the actual and a posteriori SF_6 emission rates. The left panel shows the results in WRF-DA, and the right panel shows the results in Obs-DA. The a posteriori emission rates are underestimated in WRF-DA. During the first five hours (from 9:00 to 14:00), the estimations are still within a factor two of the actual emissions, but during the last three hours (from 14:00 to 17:00), the estimations sharply drop out of the factor three. In contrast, the a posteriori SF_6 emission rates in Obs-DA are steady within a factor two of the actual emissions, except the last hour, when the estimations are underestimated. The underestimation is due to the insufficient number of observations, because only the observations from 17:00 can be used to estimate the emissions during the last hour (from 16:00 to 17:00). FAC2, NMSE and FB are calculated between the reconstructed and the actual emission rates to quantify the performance of the reconstruction. The correlation coefficient between the reconstructed and the actual emission rates is not applied, because the actual emission is almost constant during the experiment. The three statistical metrics are shown in Fig. 9. It shows that 62.5% of the estimation are within a factor two of the actual emission rates in WRF-DA, and the portion is as high as 87.5% in Obs-DA. The normalized mean square error is also larger in WRF-DA (NMSE = 0.73) than that in Obs-DA (NMSE = 0.13). The fractional bias shown in the lower panel reflects

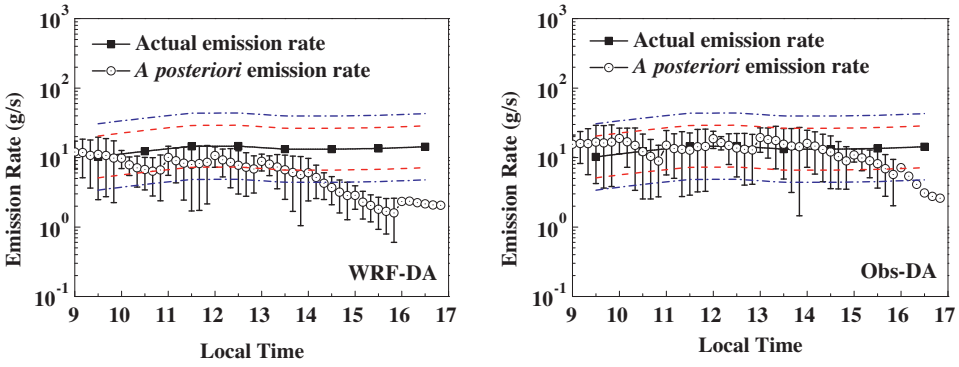

Fig. 8. The comparisons between the actual and the reconstructed emission rates: (left) results in WRF-DA, (right) results in Obs-DA. The red dashed and blue dot-dashed lines are respectively 1:2 (or 2:1) and 1:3 (or 3:1) ratio lines relative to the actual emissions. (For interpretation of the references to color in this figure legend, the reader is referred to the web version of this article.)

that the emissions are substantially underestimated in WRF-DA (FB = 0.70), but the estimations in Obs-DA are in good agreement with the actual emissions as evident in the significantly small fractional bias (FB = 0.05). WRF-Obs-DA is a new experiment, with the same configurations as WRF-DA, except that the WRF predicted boundary layer height is replaced by the height derived from the onsite meteorological measurements. The new experiment will be discussed in the next section.

3.4. Influence of boundary layer height

It is apparent that the different reconstructed emissions are caused by the meteorological data, which is the only difference between WRF-DA and Obs-DA. The DA scheme can effectively 'calibrate' the errors in the wind data as discussed in Section 3.2, hence the key influential factors must be other meteorological parameters. It is found that the height of the boundary layer exerts strong influence on the performance. In this study, the boundary layer depths (h) derived from the onsite meteorological measurements are adopted. The parameter is referred to as "derived data" hereafter. The differences of the WRF predicted and derived boundary layer heights are shown in Fig. 10. It shows that the WRF predicted boundary heights are substantially smaller than the derived data.

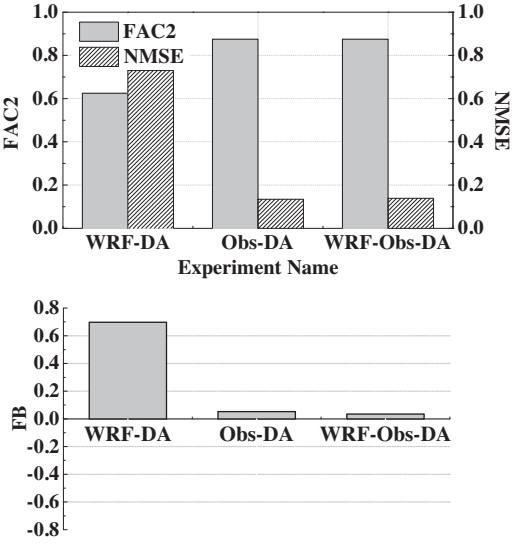

Fig. 9. FAC2 and normalized mean square error (top), fractional bias (bottom) between actual and reconstructed emission rates in WRF-DA (driven by WRF predicted data), Obs-DA (driven by WRF meteorological observations) and WRF-Obs-DA. (the same as WRF-DA, but use the observed boundary layer height).

The predictions are underestimated by 32.3% on average relative to the derived data. The largest deviations appear during the last three hours (41.5% underestimation on average). During the first hour (from 9:00 to 10:00), the predicted boundary layer heights are comparable with the derived data (within 8.5%). As a result, during that period the estimated emissions in WRF-DA are also in good agreement with the actual emission. After 14:00, the predicted heights start to decrease, but the derived data begins to nearly level off. The sharp decrease of the emission estimation in WRF-DA appears during the last three hours (from 14:00 to 17:00), as shown in the left panel of Fig. 8. Strong correlation between the deviations of the estimated emission and the deviations of predicted boundary layer height can be observed. The height of the boundary layer indicates the volume of the air that the released material can be mixed into. A lower height indicates that the released SF_6 can only be mixed into less volume of air, so the concentration after fully mixing tends to be higher. If the WRF predicted boundary layer height is lower than the "actual" value, only a reduced amount of SF_6 is required to be released in the simulation (WRF-DA) to achieve comparable concentrations with the observations. As a result, the reconstructed emissions in WRF-DA are substantially underestimated.

In order to confirm our hypothesis, a new experiment WRF-Obs-DA is designed. The new experiment is the same as WRF-DA, except that the WRF predicted boundary layer height is replaced by the height derived from the onsite meteorological measurements. Fig. 11 shows the a posteriori SF_6 emission rates in WRF-Obs-DA. The results are much better than those in WRF-DA. Fig. 9 also shows the three statistical metrics in WRF-Obs-DA. Compared with those in WRF-DA, the results in WRF-Obs-DA are drastically

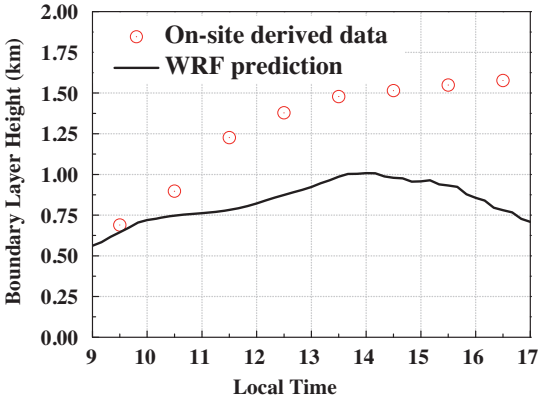

Fig. 10. Comparison between the WRF predicted and on-site derived boundary layer heights.

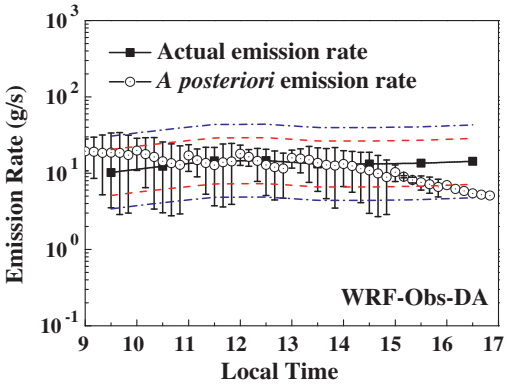

Fig. 11. Reconstructed emission rates in WRF-Obs-DA (the same as WRF-DA, except using the on-site derived boundary layer height as substitute).

improved, with a higher FAC2 (87.5%), a much smaller NMSE (0.14) and FB (0.03). The performance in WRF-Obs-DA becomes significantly close to that in Obs-DA. Since the only difference between WRF-DA and WRF-Obs-DA is the boundary layer height, it confirms that the boundary layer height is the key influential factor in the proposed EnKF data assimilation scheme.

3.5. Comparison between EnKF and iterative EnKF

The experiments WRF-Obs-DA and Obs-DA are also conducted by the original EnKF to clearly show the performance improvement of the iterative EnKF. The new experiments are respectively referred to as WRF-Obs-DA_ORIG and Obs-DA_ORIG. Fig. 12 shows the reconstructed emission rates using the original EnKF. In both of the experiments, at the initial stage of data assimilation, it takes 2 h for the original EnKF method to minimize the uncertainties of a priori parameters and converge to the actual values. In contrast, the a posteriori emission rates almost converge to the actual values during the first hour in WRF-Obs-DA and Obs-DA (seen in the right panel of Figs. 8 and 11), so the time delay of the EnKF is alleviated by the iterative EnKF.

The performance of the original EnKF scheme is also sensitive to the meteorological data. In WRF-Obs-DA_ORIG, the reconstructed emission rates deteriorate after 12:00 due to the low quality of the wind data predicted by WRF, but the results are much better in Obs-DA_ORIG due to the usage of the more accurate on-site observed meteorological data. As mentioned in Section 1, when the observational model is nonlinear, the information in measurements is not utilized maximally by the original EnKF, so the performance usually deteriorates. The different performance indicates that the original EnKF method fails to effectively correct the substantial errors in the wind data of the WRF forecasts, and the errors are reflected in the reconstructed emission rates. In contrast, the iterative EnKF is more robust and reasonably insensitive to the errors of the wind data, as evidence in the results of Obs-DA and WRF-Obs-DA. Despite using different meteorological data, the iterative EnKF scheme gives consistently high quality performance in both Obs-DA and WRF-Obs-DA (seen in the right panel of Figs. 8 and 11).

The three statistical metrics of the new experiments are shown in Fig. 13. The metrics clearly show that the emission rates reconstructed by the iterative EnKF scheme are much better than those reconstructed by the original EnKF: in Obs-DA and Obs-DA_ORIG, the FAC2 is improved by about 30%, NMSE and FB are, respectively, reduced by about 60% and 90% by the iterative EnKF scheme; in WRF-Obs-DA and WRF-Obs-DA_ORIG, the FAC2 is substantially increased by 180%, NMSE and FB are significantly cut down by about 85% and 95% by the iterative EnKF scheme.

4. Limitations and suggestions

The iterative EnKF scheme tries to simultaneously estimate the emission and improve the forecast. There is strong relation between the errors in the concentration distribution and in the wind data, so the DA scheme effectively calibrates the errors in the wind data only, which are based on the ground level concentration measurements. However it is difficult, or even impossible, to calibrate the errors in other meteorological data, such as boundary layer height, if only the observations of the ground concentrations are assimilated. The iterative EnKF scheme can not correctly identify the errors in the boundary layer height due to the error compensation effect, which means that similar ground concentration distributions can be produced under different boundary layer heights by altering the amount of the released materials. The evidence is that in WRF-DA and Obs-DA, despite the distinctly different boundary layer heights, the analysis results of ground concentrations are very close to each other (within 10% in r, and within 18% in NMSE), but the reconstructed emissions are very different. Extra constraints or observations should be introduced into the data assimilation if we want to simultaneously calibrate the errors in boundary layer height. At the current stage, for the purpose of practical application of the iterative EnKF scheme, it is suggested that the boundary layer height should be monitored near the nuclear power plant, and the data assimilation system should use the observed boundary layer height or the height derived from the meteorological measurements, namely the similar configurations as experiment Obs-DA. If the measurements are unavailable, ensemble numerical weather predictions (NWP) should be used instead of the usage of only one set of meteorological data, as suggested in [7]. The

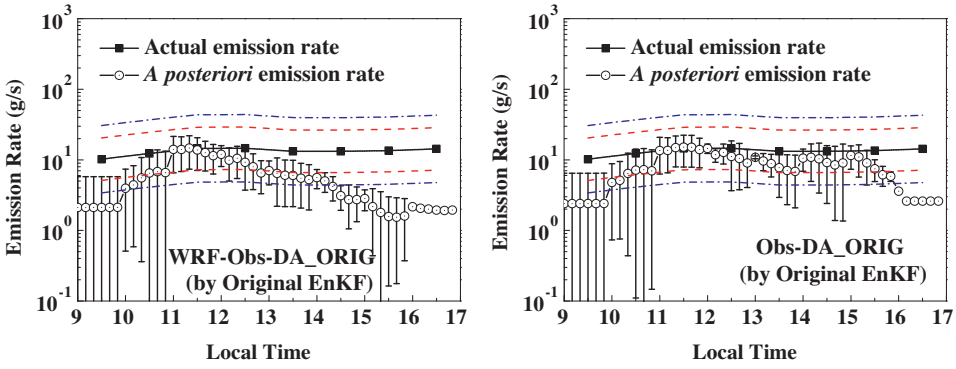

Fig. 12. Reconstructed emission rates by the original EnKF method: (left) results in WRF-Obs-DA_ORIG, (right) results in Obs-DA_ORIG. The red dashed and blue dot-dashed lines are respectively 1:2 (or 2:1) and 1:3 (or 3:1) ratio lines relative to the actual emissions. (For interpretation of the references to color in this figure legend, the reader is referred to the web version of this article.)

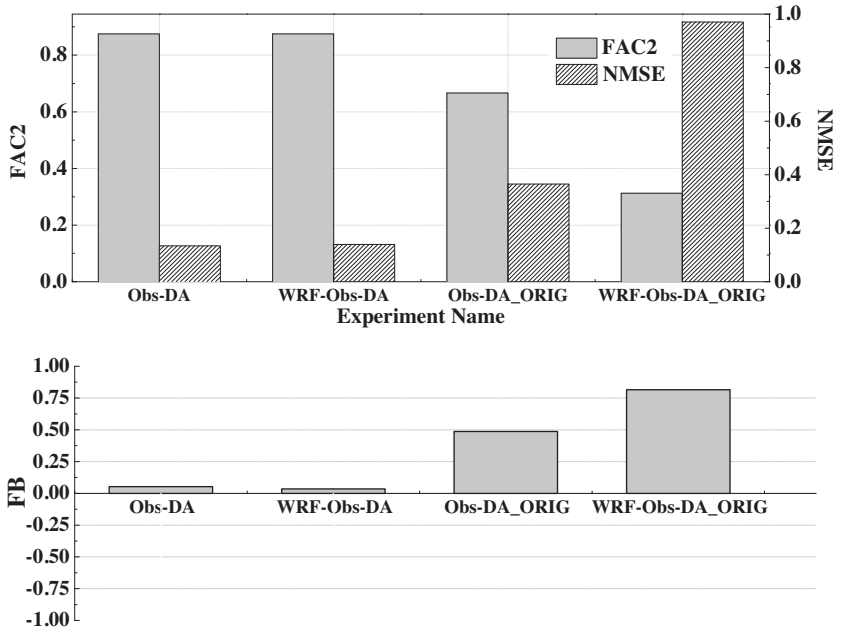

Fig. 13. FAC2 and normalized mean square error (top), fractional bias (bottom) between actual and reconstructed emission rates.

ensemble NWP data contains the information of the uncertainties in boundary layer height and other parameters, so the substantial uncertainties can be taken into account. In this study, the scenario is relatively low-wind. However, the performance of the system may also be influenced by the weather condition. For instance, when the wind speed is extremely low, the plume rise will be very high. As a result, it becomes difficult for the plume to reach the ground, which leads to the insufficiency of the measurements. On the other hand, if the wind is strong, the released puff will quickly leave the monitored area, and the monitors may fail to capture the puff. In the future study, the system will be further evaluated with the data from various weather conditions (e.g., other experiments in the Kincaid dataset).

This study is an effort toward an operational data assimilation system for nuclear emergency management. This work only focuses on the atmospheric dispersion process, and the evaluation using nonradiative tracer experiment here shows the iterative EnKF data assimilation system effectively correct the errors in the process. But in this study, the measurements are tracer concentration, which is different from the actual nuclear accident scenario, where gamma dose rate (GDR) or in situ gamma spectrometric measurements are mostly used. As a result, a new observational model should be added to convert the concentration into gamma dose rate [37], and there are some studies [11,15,38] trying to conduct data assimilation using gamma dose rate data. In order to apply the proposed iterative EnKF data assimilation method to the actual nuclear accident scenario, the following topics will be further investigated in our future study: (1) computationally efficient gamma dose rate calculation method should be developed for the Lagrangian puff model; (2) extra constraints on nuclide ratios must be introduced to reconstruct nuclide-specific source term in the situation where only gamma dose rates are available; (3) the iterative EnKF scheme is presently applicable for gaseous radionuclides, e.g., noble gas Xenon-133 and gaseous iodine, ongoing research includes extending the scheme to particulate radionuclides (e.g., Cesium-137 and particulate iodine).

The EnKF method can also be applied to correct the errors in the deposition fields at the later stages of an accident. As mentioned above, a deposition model should be added first. The contaminated fields can be described by Eulerian method, and the state vector contains the radioactive contents in each grid box [39]. Some studies [40–42] has developed EnKF data assimilation method to reconstruct the deposition field for RODOS system.

5. Conclusions

In this study, our proposed iterative EnKF data assimilation scheme in [24] is thoroughly evaluated with the data from Kincaid tracer experiment [25], which involves highly buoyant plumes. The data assimilation system is built by integrating the iterative EnKF scheme with the Lagrangian puff-model in the POLYPHEMUS platform. The data assimilation system simultaneously reconstructed the source term and improved the model forecasts.

The DA system effectively corrected the errors in the wind data (both the WRF predicted and on-site observed data), and the errors in the a priori emission rates (about six magnitudes underestimated). The DA analysis concentration (with unknown emissions) significantly outperformed the free-running dispersion models (with the actual, known SF_6 emission rates). The reconstructed emission rates had a high accuracy (87.5% within a factor two) when using the on-site observed meteorological data. However, the performance deteriorated (62.5% within a factor two) when using the WRF predicted meteorological data. The different performances were caused by the uncertainties in the boundary layer height, which is the key influential parameter in the proposed EnKF data assimilation scheme. It is suggested that the boundary layer height should be monitored near the nuclear power plant, and the substantial uncertainties in boundary layer heights should also been taken into account.

The method proposed here can be a useful tool not only in the nuclear power plant accident emergency management, but also with a little modification in the transport model in other similar situations where hazardous material is released into the atmosphere.

Acknowledgements

We thank the supports provided by National Natural Science Foundation of China (No. 91224004) and the National High-Tech

Research and Development Program of China (863 Program) (No. 2012AA050907).

References

[1] NEA, Chernobyl, Assessment of Radiological and Health Impacts–2002 Update of Chernobyl: Ten Years On in, Nuclear Energy Agency (NEA), Paris, 2002, pp. 155.
[2] NEA/OECD, The implementation of short-term countermeasures after a nuclear accident (stable iodine, sheltering and evacuation), in: Proceedings of an NEA workshop, Stockholm, Sweden, 1994.
[3] P.H. Hiemstra, D. Karssenberg, A. van Dijk, Assimilation of observations of radiation level into an atmospheric transport model: a case study with the particle filter and the ETEX tracer dataset, Atmos. Environ. 45 (2011) 6149–6157.
[4] Y. Benamrane, J.L. Wybo, P. Armand, Chernobyl and Fukushima nuclear accidents: what has changed in the use of atmospheric dispersion modeling? J. Environ. Radioactiv. 126 (2013) 239–252.
[5] A. Stohl, P. Seibert, G. Wotawa, D. Arnold, J.F. Burkhart, S. Eckhardt, C. Tapia, A. Vargas, T.J. Yasunari, Xenon-133 and caesium-137 releases into the atmosphere from the Fukushima Dai-ichi nuclear power plant: determination of the source term, atmospheric dispersion, and deposition, Atmos. Chem. Phys. 12 (2012) 2313–2343.
[6] T.J. Yasunari, A. Stohl, R.S. Hayano, J.F. Burkhart, S. Eckhardt, T. Yasunari, Cesium-137 deposition and contamination of Japanese soils due to the Fukushima nuclear accident, Proc. Natl. Acad. Sci. 108 (2011) 19530–19534.
[7] A.R. Jones, Assessing meteorological uncertainties in dispersion forecasts using a NWP Ensemble Prediction System, Int. J. Environ. Pollut. 44 (2011) 208–216.
[8] NRPB, The uncertainty in dispersion modelling estimates obtained from the working group models, NRPB Report National Radiological Protection Board, 1986.
[9] C.J.W. Twenhöfel, M.M.v. Troost, S. Bader, Uncertainty analysis and parameter optimisation in early phase nuclear emergency management, RIVM Report, National Institute for Public Health and the Environment, 2007.
[10] E. Kalnay, Atmospheric Modeling Data Assimilation and Predictability, Cambridge University Press, 2003.
[11] P. Astrup, C. Turcanu, R. Puch, C. Rojas Palma, T. Mikkelsen, Data Assimilation in the Early Phase: Kalman Filtering Rimpuff Risø National Laboratory, Roskilde, Denmark, 2004, pp. 31.
[12] C. Rojas-Palma, F. Gering, H. Madsen, R. Puch-Solis, K. Richter, H. Muller, Theoretical framework and practical considerations for data assimilation in off-site nuclear emergency management, SCK · CEN, Mol, 2001.
[13] C. Rojas-Palma, H. Madsen, F. Gering, R. Puch, C. Turcanu, P. Astrup, H. Müller, K. Richter, M. Zheleznyak, D. Treebushny, M. Kolomeev, D. Kamaev, H. Wynn, Data assimilation in the decision support system RODOS, Radiat. Prot. Dosim. 104 (2003) 31–40.
[14] M. Drews, B. Lauritzen, H. Madsen, Analysis of a Kalman filter based method for on-line estimation of atmospheric dispersion parameters using radiation monitoring data, Radiat. Prot. Dosim. 113 (2005) 75–89.
[15] M. Drews, B. Lauritzen, H. Madsen, J.Q. Smith, Kalman filtration of radiation monitoring data from atmospheric dispersion of radioactive materials, Radiat. Prot. Dosim. 111 (2004) 257–269.
[16] V. Tsiouri, I. Kovalets, S. Andronopoulos, J.G. Bartzis, Emission rate estimation through data assimilation of gamma dose measurements in a lagrangian atmospheric dispersion model, Radiat. Prot. Dosim. 148 (2012) 34–44.
[17] W. Raskob, J. Ehrhardt, C. Landman, J. PÄSler-Sauer, Status of the RODOS system for off-site emergency management after nuclear and radiological accidents, in: S. Apikyan, D. Diamond (Eds.), Countering Nuclear and Radiological Terrorism, Springer, Netherlands, 2006, pp. 151–166.
[18] R.E. Kalman, A new approach to linear filtering and prediction problems, J. Basic Eng. 82 (1960) 35–45.
[19] G. Evensen, Sequential data assimilation with a nonlinear quasi-geostrophic model using Monte-Carlo methods to forecast error statistics, J. Geophys. Res.-Oceans 99 (1994) 10143–10162.
[20] D.Q. Zheng, J.K.C. Leung, B.Y. Lee, Online update of model state and parameters of a Monte Carlo atmospheric dispersion model by using ensemble Kalman filter, Atmos. Environ. 43 (2009) 2005–2011.
[21] D.Q. Zheng, J.K.C. Leung, B.Y. Lee, An ensemble Kalman filter for atmospheric data assimilation: application to wind tunnel data, Atmos. Environ. 44 (2010) 1699–1705.
[22] D.Q. Zheng, J.K.C. Leung, B.Y. Lee, H.Y. Lam, Data assimilation in the atmospheric dispersion model for nuclear accident assessments, Atmos. Environ. 41 (2007) 2438–2446.
[23] R.J. Lorentzen, G. Naevdal, An iterative ensemble Kalman filter, automatic control, IEEE Trans. 56 (2011) 1990–1995.
[24] X.L. Zhang, G.F. Su, H.Y. Yuan, J.G. Chen, Q.Y. Huang, Modified ensemble Kalman filter for nuclear accident atmospheric dispersion: prediction improved and source estimated, J. Hazard. Mater. 280 (2014) 143–155.
[25] S.R. Hanna, R.J. Paine, Hybrid plume dispersion model (HPDM) development and evaluation, J. Appl. Meteorol. 28 (1989) 206–224.
[26] H.N. Webster, D.J. Thomson, Validation of a Lagrangian model plume rise scheme using the Kincaid data set, Atmos. Environ. 36 (2002) 5031–5042.
[27] N.E. Bowne, R.J. Londergan, Overview Results, and Conclusions for the EPRI Plume Model Validation and Development Project, Plains Site, in, EPRI Report EA-3074, 1983.
[28] I. Korsakissok, V. Mallet, Comparative study of gaussian dispersion formulas within the polyphemus platform: evaluation with prairie grass and kincaid experiments, J. Appl. Meteorol. Climatol. 48 (2009) 2459–2473.
[29] V. Mallet, D. Quélo, B. Sportisse, M. Ahmed de Biasi, É. Debry, I. Korsakissok, L. Wu, Y. Roustan, K. Sartelet, M. Tombette, H. Foudhil, Technical note: the air quality modeling system Polyphemus, Atmos. Chem. Phys. 7 (2007) 5479–5487.
[30] K.G. Brummage, The calculation of atmospheric dispersion from a stack, Atmos. Environ. (1967) 2 (1968) 197–224.
[31] A. Monin, A. Obukhov, Basic laws of turbulent mixing in the surface layer of the atmosphere, Contrib. Geophys. Inst. Acad. Sci. USSR 151 (1954) 163–187.
[32] W.C. Skamarock, J.B. Klemp, J. Dudhia, D.O. Gill, M. Barker, K.G., Duda, Y. Huang, W. Wang, J.G. Powers, A description of the Advanced Research WRF Version 3, in, 2008, pp. 1–113.
[33] E. Kalnay, M. Kanamitsu, R. Kistler, W. Collins, D. Deaven, L. Gandin, M. Iredell, S. Saha, G. White, J. Woollen, Y. Zhu, A. Leetmaa, R. Reynolds, M. Chelliah, W. Ebisuzaki, W. Higgins, J. Janowiak, K.C. Mo, C. Ropelewski, J. Wang, R. Jenne, D. Joseph, The NCEP/NCAR 40-Year Reanalysis Project, Bull. Am. Meteorol. Soc. 77 (1996) 437–471.
[34] S.-Y. Hong, Y. Noh, J. Dudhia, A new vertical diffusion package with an explicit treatment of entrainment processes, Monthly Weather Rev. 134 (2006) 2318–2341.
[35] S.-Y. Hong, J. Dudhia, S.-H. Chen, A revised approach to ice microphysical processes for the bulk parameterization of clouds and precipitation, Monthly Weather Rev. 132 (2004) 103–120.
[36] G. Evensen, The ensemble Kalman filter: theoretical formulation and practical implementation, Ocean Dyn. 53 (2003) 343–367.
[37] S. Andronopoulos, J.G. Bartzis, A gamma radiation dose calculation method for use with Lagrangian puff atmospheric dispersion models used in real-time emergency response systems, J. Radiol. Prot. 30 (2010) 747–759.
[38] V. Smidl, R. Hofman, Efficient sequential monte carlo sampling for continuous monitoring of a radiation situation, Technometrics 56 (2014) 514–527.
[39] X.L. Zhang, Q.B. Li, G.F. Su, M.Q. Yuan, Ensemble-based simultaneous emission estimates and improved forecast of radioactive pollution from nuclear power plant accidents: application to ETEX tracer experiment, J. Environ. Radioact. 142 (2015) 78–86.
[40] F. Gering, Data assimilation methods for improving the prognoses of radionuclide deposition from radioecological models with measurements, in: Institute for Ion Physics, The University of Innsbruck, Innsbruck, Austria, 2005, pp. 151.
[41] F. Gering, K. Richter, H. Muller, Combination of measurements and model predictions after a release of radionuclides, Kerntechnik 69 (2004) 243–247.
[42] F. Gering, W. Weiss, E. Wirth, R. Stapell, P. Jacob, H. Muller, G. Prohl, Assessment and evaluation of the radiological situation in the late phase of a nuclear accident, Radiat. Prot. Dosim. 109 (2004) 25–29.